

This article may be downloaded for personal use only. Any other use requires prior permission of the author and AIP Publishing. This article appeared in Bingyang Zhang, Glenn S. Solomon, Matthew Pelton, Jocelyn Plant, Charles Santori, Jelena Vučković, Yoshihisa Yamamoto; Fabrication of InAs quantum dots in AlAs/GaAs DBR pillar microcavities for single photon sources. Journal of Applied Physics 1 April 2005; 97 (7): 073507. <https://doi.org/10.1063/1.1882764> and may be found at <https://doi.org/10.1063/1.1882764>.

Access to this work was provided by the University of Maryland, Baltimore County (UMBC) ScholarWorks@UMBC digital repository on the Maryland Shared Open Access (MD-SOAR) platform.

Please provide feedback

Please support the ScholarWorks@UMBC repository by emailing scholarworks-group@umbc.edu and telling us what having access to this work means to you and why it's important to you. Thank you.

RESEARCH ARTICLE | MARCH 21 2005

Fabrication of InAs quantum dots in AlAs / GaAs DBR pillar microcavities for single photon sources

Bingyang Zhang; Glenn S. Solomon; Matthew Pelton; Jocelyn Plant; Charles Santori; Jelena Vučković; Yoshihisa Yamamoto



Journal of Applied Physics 97, 073507 (2005)

<https://doi.org/10.1063/1.1882764>



View
Online



Export
Citation

CrossMark

Articles You May Be Interested In

Single and Coupled Microcavities — AlAs/GaAs DBR Pillars and GaAs Pyramids

AIP Conference Proceedings (April 2007)

Enhanced single-photon emission from a quantum dot in a micropost microcavity

Appl. Phys. Lett. (May 2003)

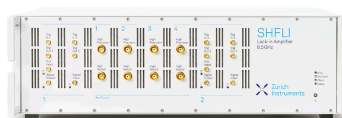
Correlated photon pairs from single (In, Ga)As/GaAs quantum dots in pillar microcavities

Journal of Applied Physics (December 2004)

500 kHz or 8.5 GHz?

And all the ranges in between.

Lock-in Amplifiers for your periodic signal measurements



Find out more

 Zurich
Instruments

Fabrication of InAs quantum dots in AlAs/GaAs DBR pillar microcavities for single photon sources

Bingyang Zhang,^{a)} Glenn S. Solomon,^{b)} Matthew Pelton,^{c)} Jocelyn Plant, Charles Santori,^{d)} Jelena Vučković, and Yoshihisa Yamamoto^{e)}

Quantum Entanglement Project, ICORP, JST, Edward L. Ginzton Laboratory, Stanford University, Stanford, California 94305-4085

(Received 1 November 2004; accepted 7 February 2005; published online 21 March 2005)

We report the molecular beam epitaxy growth of low-density strain-induced InAs quantum dots (QD) embedded in an AlAs/GaAs distributed Bragg reflector structure for a triggered photon source. By optimal selection of growth temperature, InAs deposited thickness and other experimental parameters, it is possible to grow low density ($10/\mu\text{m}^2$) InAs quantum dots with a suitable emission wavelength for a triggered photon source. The empirical formulas for the refractive indices of AlAs and GaAs materials at high temperature over a wide wavelength range are constructed by combining high resolution x-ray diffraction, dynamic optical reflectivity, and optical reflectivity spectrum techniques. Utilizing the electron-beam lithography and electron-cyclotron-resonance plasma etching techniques, a micropost microcavity with the top diameter of $0.6\ \mu\text{m}$ and the post height of $4.2\ \mu\text{m}$ has been fabricated. Narrow, spectrally limited single QD emission embedded in a micropost microcavity is observed in the photoluminescence.

© 2005 American Institute of Physics. [DOI: 10.1063/1.1882764]

I. INTRODUCTION

Since it was proposed that three-dimensional confinement of an electron-hole pair to a region smaller than the de Broglie wavelength could enhance light emission,¹ some interesting applications for quantum dots (QDs) have been studied, such as QD lasers,²⁻⁴ single electron memories,⁵ and single-photon emitters.⁶⁻¹⁰

The three-dimensional confinement of the many-body electron-hole states results in an energy spectrum consisting of a series of discrete lines. The cascade biexcitonic and excitonic emission of two photons from two electron-hole pairs features slightly different emission wavelengths due to Coulomb interactions among charged carriers. With this property of QD emission, we can realize a single-photon source and entangled photon source.⁶⁻¹⁰ An efficient source of single-photon is useful for quantum key distribution and quantum computation.¹¹⁻¹³ If we put the QDs in a planar dielectric microcavity, the emission properties can be modified. Spontaneous emission in the normal direction is enhanced if the cavity is resonant with the emission and the QDs are located at an antinode position of a cavity field, while if there is no coupling to other modes the spontaneous emission is inhibited if the cavity is off resonant and/or the QDs are located at a node position. Due to the enhanced emission coupling into a single cavity mode, the spontaneous

emission will have a good directionality, and thus can be more easily coupled into the downstream optical components. For the realization of such enhanced spontaneous emission, we first epitaxially grow InAs QDs embedded in a GaAs optical cavity layer using molecular beam epitaxy (MBE). Then, we put this cavity inside multilayer distributed Bragg reflectors (DBR) for enhancing the emission more, which can also be finished by the MBE technique. At last, a single QD buried between DBR structures can be isolated by electron-beam lithography (EBL) and reactive ion etching methods. If the QD density is small enough, for instance $<10^9$ dots/cm², we can isolate 1–2 QDs within a $0.5\ \mu\text{m}$ micropost.

The growth of low-density QDs is a first step to realize such a single-photon source. Since the first growth of In-GaAs quantum dots (QDs) by self-organized model,¹⁴ there has been intensive QD growth mechanisms studies.¹⁵⁻²⁰ Interest continues to focus on controlling the uniformity of the dot size, density, and optical emission properties. For example, for the fabrication of QD lasers, the growth of high density QD ($>10^{11}$ dots/cm²) is important. However, for single-photon source applications, it is essential to grow QDs with low density ($\sim 10^9$ dots/cm²). Although, there are some reports which discuss the effects of coverage, flux, substrate temperature, and growth rate on the formalization of high density InAs QDs,²¹⁻²³ far less attention and discussion have been paid to the study for the formation of low density QD.

In this work, we first study the growth of InAs QDs with low density using MBE. Atomic force microscopy (AFM) and photoluminescence (PL) measurements are carried out to characterize the QD size, uniformity, density, and optical properties. The effects of growth temperature and InAs coverage on the size and density have been mainly investigated.

^{a)}Electronic mail: byzhang@stanford.edu

^{b)}Also at Solid State Photonics Laboratory, Stanford University, Stanford, California 94305-4085.

^{c)}Current address: James Franck Institute, 5640 South Ellis Avenue, University of Chicago, Chicago, Illinois 60637.

^{d)}Also at: Institute of Industrial Science, The University of Tokyo, 4-6-1, Komaba, Meguro-ku, Tokyo 153-8505, Japan.

^{e)}Also at: NTT Basic Research Laboratories, Atsugi, Kanagawa 243-0198, Japan.

Low-density InAs QDs, with density of about $10/\mu\text{m}^2$, has been grown by suitably controlling the experimental conditions.

Moreover, we focus on controlling the epitaxial thickness of AlAs/GaAs DBR structures. In general, thickness control with better than 1% accuracy is needed for successfully achieving the desired optical properties of DBR structure.²⁴ Accurately controlling the growth thickness requires wavelength and temperature-dependent knowledge of the refractive indices of semiconductor materials. By combining high resolution x-ray diffraction (HRXRD) and optical reflectivity spectrum measurements, we obtain empirical formulas for the refractive indices of AlAs and GaAs at a high temperature over the necessary wavelength range for our AlAs/GaAs DBR structures.

Finally, we fabricate the micropost microcavity with EBL and electron-cyclotron-resonance (ECR) plasma etching. Photoluminescence experiment was employed to examine the resonance photon emission of the cavity.

II. GROWTH OF LOW-DENSITY InAs QDs BY MBE

The formation mechanisms of InAs QDs on the GaAs layer grown with MBE are generally explained by the Stranski–Krastanov (SK) mode.²⁵ When In and As fluxes impinge on the GaAs, the lattice-mismatch strain energy is initially low and the InAs deposits as a rough planar layer called the wetting layer. Future deposition generates an adatom layer, from which two-dimensional (2D) surface morphology (or called 2D islands) nucleates on the top of the wetting layer. However, as deposition continues, the accumulated strain energy induced by the 7% lattice mismatch between GaAs and InAs can not relieve totally in the 2D directions islands. Instead, three-dimensional (3D) islands form, which the strain energy can relieve through their top and sidewalls. Several theoretical descriptions have been developed to model the SK growth mechanisms,^{26–33} including those based on thermal-equilibrium,^{29,30} and those that emphasize the kinetic role on the formation of QDs.^{31–33} In the kinetic model, the process of the formation of QDs is divided into four steps, i.e., atoms deposition on the growth surface; adatom diffusion over the surface; attachment and detachment; and 2D–3D transition.

The InAs QD samples studied here were grown on semi-insulating (100) epi-ready GaAs substrates in a Varian GEN-II MBE system. A wafer was first baked at the temperature of about 400 °C for around 1.5 h before being loaded into the growth chamber. A 10 keV reflection high-energy electron diffraction (RHEED) system was used to monitor the reconstruction of the GaAs wafer surface when heating it for deoxidization and also used to calibrate the growth temperature. A 0.3 μm GaAs buffer layer was grown in each sample at 570 °C in order to smooth the surface. We grow two layers of QDs separated by an 800 Å GaAs layer, one of which is left exposed on the surface (for AFM). Here we notice it is not so straightforward to compare properties between the upper and lower QD layer due to the top QD layer without the capping layer. We changed the growth temperature and InAs coverage to study their effects on the QD

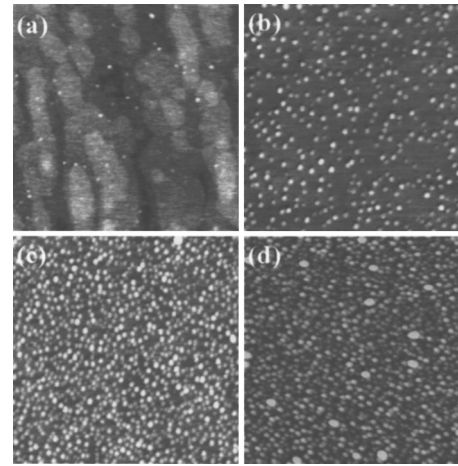


FIG. 1. AFM images of InAs QDs grown on (100) GaAs substrate at coverage of (a) 1.74, (b) 1.89, (c) 2.03, and (d) 2.61 MLs. The growth temperature is 475 °C. The measured area is $1 \times 1 \mu\text{m}^2$.

size, density and optical properties. The growth rate and the ratio of As to In were kept at 0.07 ML/s and 50, respectively, for all the samples.

The AFM measurements are performed *ex situ* with a Nanoscope III from Digital Instrument in contact mode. The evolution of the density and the in-plane diameter of InAs/GaAs QDs with different coverage are shown in Fig. 1. The $1.0 \times 1.0 \mu\text{m}^2$ AFM images are obtained from the coverage of 1.74, 1.89, 2.03, and 2.61 MLs InAs QD samples, respectively. Here, the growth temperature for InAs deposition is 475 °C. As is the typical case Fig. 1 shows that the QD island density increases with increasing coverage. Because of their comparably small size and density, the QD islands in Fig. 1(a) with coverage of 1.74 ML appear to be just beyond the 2D to 3D transition. With the increase of coverage, the formation of 3D InAs QD islands evolves over the entire wetting layer surface uniformly. When the coverage arrives to 2.6 ML, Fig. 1(d), some coalescence appears.

A summary of density, height, and base diameter of the QDs measured by AFM are shown in Figs. 2 and 3. Figure 2 shows that large InAs coverage leads to high InAs QD density, while the lowest density of InAs QDs ($\sim 10^9/\text{cm}^2$) can be obtained with about 1.74 ML. When the coverage increases, the density sharply increases. Once the coverage exceeds about 2 ML, the formation speed of QD density de-

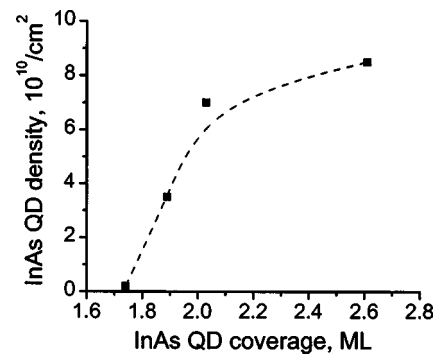


FIG. 2. The dependence of the density of the InAs QDs on the InAs coverage grown on GaAs substrate by MBE.

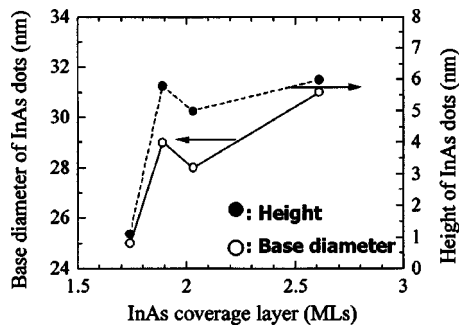


FIG. 3. The dependencies of InAs QD height and base diameter on the InAs coverage.

creases, and seems to saturate. The saturation of density may come from two aspects. As soon as 3D islands nucleate, they act as capture center not only for adatoms that are deposited but also for those atoms detaching from 2D islands. Thus, the 2D island size decreases, which causes reduction of the conversion rate of the 2D island to 3D island. Hence, the initially large rate of QD island formation decreases. The other reason is due to the coalescence of 3D islands at thick coverage layer. Both processes produce the same general result. The evolution trends of the base diameter and height of the InAs QDs with the coverage layer give the same result. Both the base diameter and the height arrive at the largest value for 1.89 ML coverage. Along with the increase of the coverage, the diameter and the height trend to saturation. Here, we notice that we can grow the QD density as high as $9 \times 10^{10}/\text{cm}^2$, and such high density is hopeful in QD laser fabrication.

While low QD island density is obtained at low coverage at constant substrate temperature, the QD island size also decreases. The smaller sizes of QDs limit the emission efficiency and intensity, and cause an unexpected emission wavelength in the fabrication of triggered photon sources. Adjusting the growth temperature also affects the QD density and optical properties. Keeping the InAs coverage in the range of 1.9 ML, we can, in the future, adjust the QD size and density by changing the growth temperature. This method lets us obtain relative low-density distribution with larger sizes.

Figure 4 shows the experimental results of the variation of InAs QD density with the change of the InAs QD growth temperature at 1.89 ML InAs coverage. Under the high growth temperature, we obtain the lowest InAs island density ($\sim 20/\mu\text{m}^2$), while the height and base diameter of InAs QDs increase with the temperature, which shows a trend of low density-large size. During SK growth with kinetic model, adatoms adsorbing to the wetting layer from deposition process are assumed the only mobile surface species. Diffusion adatoms meet bond together and form small 2D islands. Mobile adatoms hop randomly on the InAs wetting layer around nearest-neighbor sites dependent on the surface diffusion constant,^{34,35} which is mainly decided by the growth temperature. The increase of the growth temperature enhances the mobility of In adatoms on the InAs wetting layer surface, which decreases the accumulation of atoms on the top of 2D islands. Hence, the speed of conversion of 2D islands to 3D islands would decrease.

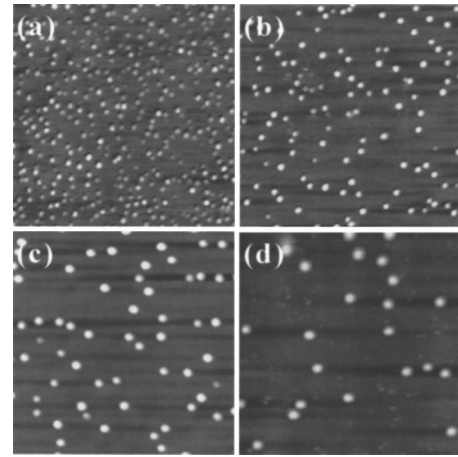


FIG. 4. AFM images of InAs QDs grown on (100) GaAs substrate with 1.89 ML InAs coverage by MBE at growth temperatures of (a) 475, (b) 482, (c) 505, and (d) 525 °C. The growth rate of InAs QDs is 0.07 ML/s, and ratio of As to In is about 50. The measured area is $1 \times 1 \mu\text{m}^2$.

Figure 5 shows the experimental results of the relationship between the InAs QD density and the growth temperature (shown by circles). The InAs coverage is 1.89 ML, and the growth temperature changes from 460 °C to 525 °C. Under these growth conditions, there is an abrupt change in the QD density. At low growth temperatures QD formation is inhibited by poor kinetics, while kinetic barriers are removed as the growth temperature increases. In the high temperature regime there is a narrow window where low density with relatively large QDs can be made. According to a simple thermally activated diffusion equation, the 3D island density (n_d) is proportional to temperature: $n_d \propto (2h/kT)^{1/3} \cdot (G/a_0)^{1/3} \cdot \exp[E_f(T)/3kT]$,^{34–36} where h and k are the Planck's and the Boltzmann's constants, a_0 is the distance of a nearest-neighbor hopping, $E_f(T)$ is the energy barrier, T is the growth temperature, and G is the growth rate with unit of monolayer/s. With this formula, we can explain the dependence of InAs QD density on growth temperature in partially temperature regime, separately. The abrupt reduction in the density with increased growth temperature indicates an additional process besides simple thermally activated kinetics. One possibility is interdiffusion of gallium atoms into the InAs QDs by a temperature-dependent segregation during growth. The interdiffusion of the gallium atoms

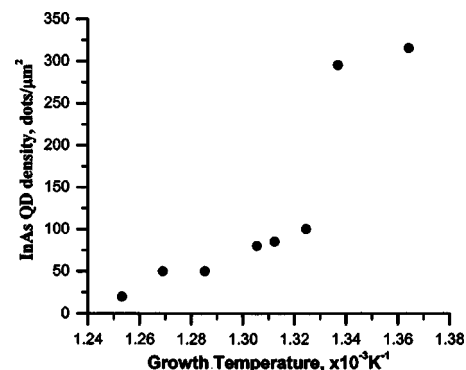


FIG. 5. The dependence of the InAs QD density, grown on GaAs (100), on the inverse of the growth temperature at the growth rate of 0.07 ML/s and an As/In ratio of 50.

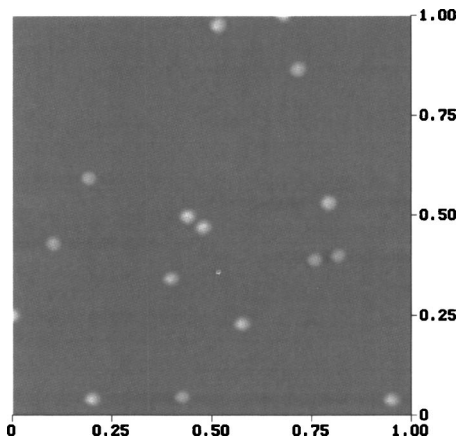


FIG. 6. Low-density InAs QD distribution grown by MBE with 1.81 ML coverage. The measured area is $1 \times 1 \mu\text{m}^2$.

into the InAs QDs would result the formation of InGaAs QDs, which causes the strain reduction. According to the elasticity theory,³⁷ the change of the barrier due to the strain is proportional to the strain. Thus, we expect a low energy barrier value for fit at high growth temperature.

Figure 6 shows our result with low-density InAs QD distribution obtained under 1.81 ML InAs coverage and growth temperature of 525 °C. The InAs QD density is about $10/\mu\text{m}^2$, and the height and the base diameter of the QDs measured by AFM are about 2 nm and 30 nm, respectively. These experimental conditions were used in growing single-photon emission source with DBR structure.

III. PL CHARACTERISTICS OF QDs

PL measurements were carried out at low temperature (4 K) for different InAs QD growth temperatures. A mode-locked Ti:sapphire laser which was pumped by a solid-state diode-pumped laser (Model: Verdi™ V-10) and emitted 1 ps pulses with a repetition rate of 76 MHz was used. A lens was used to focus the pump laser beam to a $\sim 5 \mu\text{m}$ diameter spot on the sample. The PL was focused onto a pinhole that effectively selected a $3 \mu\text{m}$ region of the sample, and rejected scattered laser light. The light signal was then detected by a liquid nitrogen cooled CCD array camera following a spectrometer with 1 Å spectral resolution.

Figure 7 shows the PL experimental results at the growth temperatures 450, 482, 493, and 515 °C, respectively. Bro-

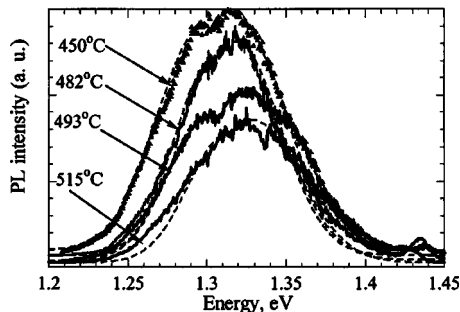


FIG. 7. Low temperature (4 K) PL emission spectra obtained from InAs/GaAs QD samples grown on a GaAs substrate at temperature of 450, 482, 493, and 515 °C.

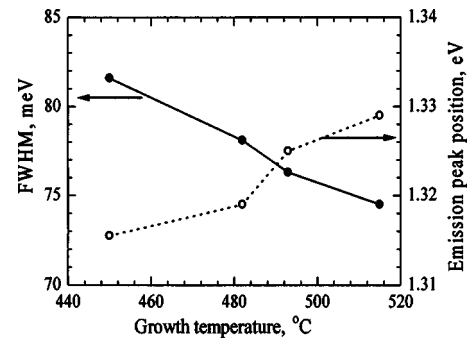


FIG. 8. Temperature dependence of emission peak position and the FWHM for InAs QD.

ken lines are the Gaussian fitting of each peak. Due to the fluctuation of QD sizes and shapes that lead to a variation in the confined energy levels, the QD ensemble emits a broad peak in PL spectra. Moreover, the distinctive double-peaks can be seen from PL spectra, especially at low growth temperature. When the growth temperature increases the double-peak gradually becomes together. In addition, the energy peak position of QD ensemble emission in the PL spectra changes to high direction with the increase of the growth temperature (Fig. 8). A possibility may be due to the interdiffusion of Ga atoms into the InAs QDs at high temperature. From Fig. 8, a concomitant narrowing of full-width at half-maximum (FWHM) from 82 meV to 74 meV with the increase of the growth temperature reveals a narrower QD size distribution at high temperature.

Besides the uniform QD size, shape, and the interdiffusion of Ga atoms into InAs QD, the sparse QD distribution partly contributes to the decrease of FWHM. From the AFM image of Fig. 4, we can see the distances between vicinal QDs increase with the temperature. The value gradually becomes larger than 100 nm, which leads to the reduced weak coupling between QDs. So, a large amount of QDs are decoupled from each other, and the efficient relaxation process of carriers will happen inside each QD. Figure 9 shows the relationship between the QD density and FWHM. It clearly displays the variation trend, i.e., low QD density leads to narrow FWHM. The insert PL picture in Fig. 9 shows a well uniform QD size and shape sample with a low density of about $20/\mu\text{m}^2$. The dotted line is a Gaussian fitting result. A very narrow FWHM of around 17 meV is obtained from such sample.

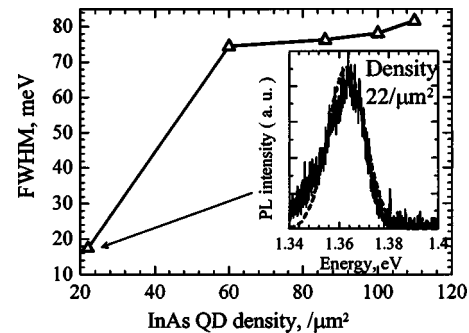


FIG. 9. Dependence of FWHM on the InAs QD density. A narrow linewidth of 17 meV is obtained from the density of $20/\mu\text{m}^2$.

IV. GROWTH OF AIAs/GaAs DBR STRUCTURES

The designed structure of triggered photon source includes a GaAs cavity region consisting of 1.81 ML of InAs QDs in the middle. The cavity thickness corresponds to one-wavelength at the cavity resonance. The bottom and the top mirrors of the cavity are the DBR layers consisting of quarter-wavelength thick AIAs/GaAs layers. The bottom DBR has 35.5 pairs, while the top has 16 pairs. That the bottom DBR reflectivity is higher than the top DBR is to let almost all of the emission light in the cavity escaping upwards rather than downwards. The resonance wavelength is designed to coincide with the photon emission peak of InAs QDs.

Controlling the growth thickness and crystal quality of DBR layers is important for successfully achieving the desired optical properties of DBR structure. The methods of optical reflection difference³⁸ and dynamic optical reflectivity³⁹ are typically used to measure the growth rate in MBE experiment. To calculate the growth rate, using these techniques, the refractive index at high temperature is needed. The refractive indices are sensitive to the temperature and the wavelength of light. Unfortunately, the refractive indices at high temperature for AIAs and GaAs over a sufficient wavelength region are not well known. In our experi-

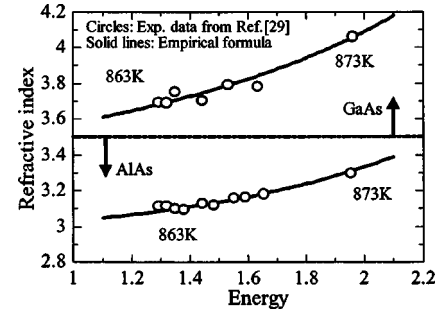


FIG. 10. The dependence of the refractive indices of GaAs and AIAs on the energy at high temperature.

ment, they are achieved by combining *in situ* optical reflectivity and *ex situ* high-resolution x-ray diffraction (HRXRD). Based on the above experimental data, we constructed the empirical formulas for the refractive indices of AIAs and GaAs at high temperature over a relative wide wavelength range.

Figure 10 shows the dependence of the refractive indices of GaAs and AIAs on the energy at temperature of 873 K. Circles are the experimental data,⁴⁰ and solid lines are the empirical formulas according to the following equations:⁴¹

$$n(T, \lambda)_{\text{GaAs}} = \sqrt{A(T)_{\text{GaAs}} + \frac{10^{-8}}{E_0^2(T) - (hc/\lambda)^2} + \frac{9.404}{E_1^2(T) - (hc/\lambda)^{0.96}}} \quad (1)$$

and

$$n(T, \lambda)_{\text{AIAs}} = \sqrt{A(T)_{\text{AIAs}} + \frac{0.0609}{E_0^2(T) - (hc/\lambda)^2} + \frac{61.064}{E_1^2(T) - (hc/\lambda)^{2.23}} + R(\lambda)}, \quad (2)$$

where T is the temperature, λ is the wavelength, h is the Planck constant, and c is the optical speed. $E_0(T)$ is set to be the band gap energy, E_g , whose temperature dependence is⁴²

$$E_0(T) = E_0(0) + 2.862 \cdot 10^{-2} \cdot \left[1 - \coth\left(\frac{1.59 \cdot 10^{-2}}{2k_B T}\right) \right] + 3.696 \cdot 10^{-2} \cdot \left[1 - \coth\left(\frac{3.39 \cdot 10^{-2}}{2k_B T}\right) \right], \quad (3)$$

where k_B is the Boltzmann constant, $E_0(0) = 1.5192$ for GaAs and 3.099 for AIAs. The energy $E_1(T)$ and $A(T)$ are assumed to depend on the temperature by the following formulas:

$$A(T)_{\text{GaAs}} = 7.3377 + 5.534 \cdot 10^{-4} \cdot T - 3.56 \cdot 10^{-7} \cdot T^2, \quad (4)$$

$$A(T)_{\text{AIAs}} = 2.857 + 4.574 \cdot 10^{-4} \cdot T - 2.942 \cdot 10^{-7} \cdot T^2, \quad (5)$$

$$E_1^2(T) = E_1(0) - 3.779 \cdot 10^{-4} \cdot T - 1.121 \cdot 10^6 \cdot T^2, \quad (6)$$

where $E_1(0) = 3.791$ for GaAs and 11.717 for AIAs. For GaAs $R(\lambda) = 0$, and for AIAs

$$R(\lambda) = \frac{2.157 \cdot 10^{-3}}{1.331 \cdot 10^{-3} - (hc/\lambda)^2}. \quad (7)$$

Figure 11 shows a HRXRD measurement by (004) scan using a Philips X'Pert HRXRD instrument to 20 pairs of GaAs and AIAs on a 0.3 μm GaAs buffer layer grown at 590 °C. The experimental rocking curve is shown in Fig. 11(a). The high number of visible satellite peaks indicates the high crystalline quality of DBR structure. Figure 11(b) shows the simulation result by using commercial software (Philips X'Pert Epitaxy Analysis Software). We can get a good agreement between experimental data and simulation results. The standard deviation in thickness for GaAs and AIAs is 1%. The effect of the changes of the lattice parameters with the growth temperature was also considered in the calculation. Moreover, we carried out the optical reflectivity

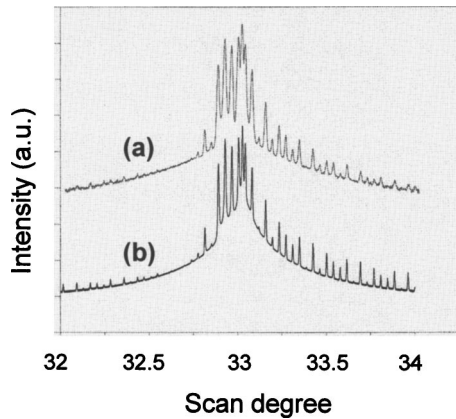


FIG. 11. Experimental HRXRD curve (a), and simulation curve (b) for 20 pairs of a GaAs/AlAs DBR structure.

spectrum (ORS) measurement at room temperature to check up the thickness further.⁴³ We found the calculated ORS results to be in a good agreement with the experimental data on the bandpass and in a long wavelength region. This agreement confirms the accuracy of the thickness obtained from the HRXRD measurement. With this method, the accuracy of DBR structure thickness can be controlled around 1%. We expect our empirical formulas for GaAs and AlAs to be of several uses in a variety of optical device structures.

V. FABRICATION OF MICROPOST

After the successfully growth of the cavity structure containing InAs QDs at the center antinode, and surrounded by the AlAs/GaAs DBR pairs, the fabrication of micropost is achieved by employing EBL and dry etching. For EBL, we used a Leica Stereoscan 440 SEM. Writing software Nanometer Pattern Generation System produced by J. C. Nabit was used for lithographic patterns. During the writing, optimal choice of electron beam current and energy, magnification and exposure dose was experimentally decided to meet the requirement on the resolution and saving the exposure time.

A bilayer resist was used in the etching. This bilayer consists of a top layer of low-sensitive PMMA and lower layer of high-sensitive copolymer of MMA and methacrylic acid (P(MMA-MAA)). A mixture of a polar and a nonpolar solvent develops both layers simultaneously, which will improve the undercut profile etching. A thick Ni layer (~ 100 nm) was deposited on the sample as a mask for deep etching of microposts.

Dry etching was carried out by using a low-pressure electron-cyclotron-resonance plasma etcher (PlasmaQuest) with a dilute mixture of Cl_2 and BCl_3 in a background of Ar. The sample was cooled by flowing helium gas at about 3°C . The etching process was divided into three steps. In each subsequent step, we decreased the partial pressure of Cl_2 and the process pressure. While, the applied rf power was increased to maintain a roughly constant dc bias. The adoption of three steps during the etching is helpful in improving the undercut profile.

Figure 12 shows a scanning electron microscope (SEM) image of a typical etched micropost. The top diameter of the post is $0.6\ \mu\text{m}$, and the height is around $4.2\ \mu\text{m}$. The

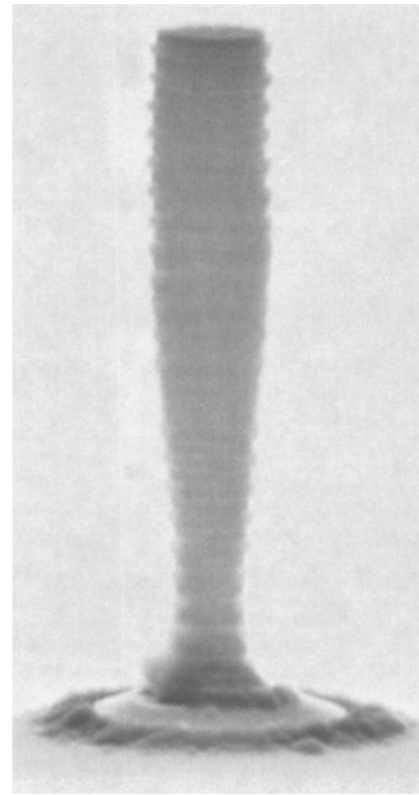


FIG. 12. A SEM image of a typical micropost microcavity, constructed of GaAs/AlAs DBR pairs with InAs QDs buried in the center of the GaAs cavity. The top diameter is $0.6\ \mu\text{m}$, and the height is $4.2\ \mu\text{m}$.

AlAs/GaAs DBR structures are clearly visualized as dark and white areas, respectively. The one-optical wavelength GaAs cavity region is also shown clearly in the near middle area in the micropost. Although we have used bilayer resists, cooling the sample and dividing the etching process into three steps during the etching, undercut profile is still present, but can be improved in the future.

VI. OPTICAL CHARACTERIZATION OF MICROPOST MICROCAVITY

Using the above mentioned for growth and etching, we fabricated micropost microcavities for triggered photon sources. The optical experimental set-up to the micropost microcavities is the same as that in PL experiment to the QDs except the addition of a Hanbury Brown and Twiss (HBT) type apparatus for measuring the photon correlation function. The sample is set in a liquid helium cryostat at the temperature of about $4\ \text{K}$. The emitted photon light can be sent to a spectrometer, a streak camera or be directed towards the HBT for measuring the intensity as a function of time and of wavelength, or to record a histogram of time intervals between photons. More detail on the experimental methods can be found in Refs. 44 and 45.

Figure 13 shows the PL experimental result from a micropost microcavity containing a single InAs quantum dot. The emission in the wavelength range of $835\text{--}845\ \text{nm}$ is from the wetting layer. Spectrally isolated emission at a wavelength of $855\ \text{nm}$ is due to a single quantum dot. The fundamental resonance wavelength of the cavity is designed at a near-resonant wavelength of $855\ \text{nm}$. This QD emission

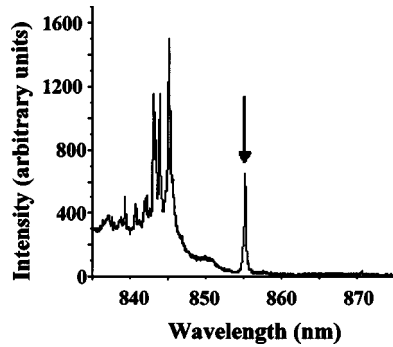


FIG. 13. Photoluminescence from a micropost microcavity containing a single InAs quantum dot.

line is used in our single photon emission studies. The certification of single photon emission was experimentally carried out by measurement of photon correlation function $g^{(2)}(\tau)$. The experimental value of quality factor Q for such sample is round 600. The detail expressions on the experimental set-up and discussions on the experimental results can be found in Refs. 44 and 45. The measured normalized second-order correlation function shows the normalized central peak area is as low as 0.10 under the incident pump power of $10.9 \mu\text{W}$. This is a clear indication of strong antibunching for the emitted photons, and demonstrates that a triggered single photon has been achieved.

VII. SUMMARY

The achievement of an efficient, single photon source is a basic condition in the quantum communication.^{46,47} By employing the nanofabrication and the material growth techniques, we have fabricated such a single photon source. A micropost microcavity with a low density of InAs QDs positioned at the antinode of a wavelength-thick GaAs cavity layer surrounded by AlAs/GaAs DBR pairs has been fabricated. We have demonstrated a strong dependence of InAs QD density on the growth temperature in the MBE growth. With an increase of the growth temperature, the emission wavelength moves to a shorter wavelengths, and the FWHM becomes narrower due to more uniform size and shape distribution. A set of empirical formulas for the refractive indices of GaAs and AlAs at a high temperature have been developed over a wide wavelength range, allowing us to precisely control the thickness of AlAs and GaAs DBR layers. The PL data from the micropost microcavity features the resonant emission of an isolated single InAs QD with the cavity.

¹Y. Arakawa and H. Sakaki, *Appl. Phys. Lett.* **40**, 939 (1982).

²N. Kirstaedter, N. N. Ledentsov, M. Grundmann, D. Bimberg, V. M. Ustinov, S. S. Ruvimov, M. V. Maximov, P. S. Kop'ev, Zh. I. Alferov, U. Richter, P. Werner, U. Gösele, and J. Heydenreich, *Electron. Lett.* **30**, 1416 (1994).

³Matthew Pelton and Yoshihisa Yamamoto, *Phys. Rev. A* **59**, 2418 (1999).

⁴J. A. Lott, N. N. Ledentsov, V. M. Ustinov, N. A. Maleev, A. E. Zhukov, A. R. Kovsh, M. V. Maximov, B. V. Volovik, Zh. I. Alferov, D. Bimberg, *Electron. Lett.* **36**, 1384 (2000).

⁵K. Yano, T. Ishii, T. Hashimoto, T. Kobayashi, F. Murai, and K. Seki, *IEEE International Electron Device Meeting, Technical Digest*, 1993, p. 541.

⁶P. Michler, A. Kiraz, C. Becher, W. V. Schoenfeld, P. M. Petroff, Lidong

Zhang, E. Hu, and A. Imamoglu, *Science* **290**, 2282 (2000).

⁷C. Santori, M. Pelton, G. Solomon, Y. Dale, and Y. Yamamoto, *Phys. Rev. Lett.* **86**, 1502 (2001).

⁸G. S. Solomon, M. Pelton, and Y. Yamamoto, *Phys. Rev. Lett.* **86**, 3903 (2001).

⁹E. Moreau, I. Robert, J. M. Gérard, I. Abram, L. Manin, and V. Thierry-Mieg, *Appl. Phys. Lett.* **79**, 2865 (2001).

¹⁰O. Benson, C. Santori, M. Pelton, and Y. Yamamoto, *Phys. Rev. Lett.* **84**, 2513 (2000).

¹¹C. H. Bennett and G. Brassard, in *Proceedings of the IEEE International Conference On Computational Systems and Signal Processing*, Bangalore, India, 1984, p. 175.

¹²I. Chang and Y. Yamamoto, *Phys. Rev. A* **52**, 3489 (1995).

¹³E. Knill, R. Laflamme, and G. L. Milburn, *Nature (London)* **409**, 86 (2000).

¹⁴L. Goldstein, F. Glas, J. Y. Marzin, M. N. Charasse, and G. Le Roux, *Appl. Phys. Lett.* **47**, 1099 (1985).

¹⁵D. Leonard, M. Krishnamurthy, C. Reaves, S. P. Denbaars, and P. M. Petroff, *Appl. Phys. Lett.* **63**, 3203 (1993).

¹⁶J. M. Moison, F. Houzay, F. Barthe, L. Leprince, E. André, and O. Vatel, *Appl. Phys. Lett.* **64**, 196 (1994).

¹⁷G. S. Solomon, J. A. Trezza, and J. S. Harris, Jr., *Appl. Phys. Lett.* **66**, 991 (1995).

¹⁸S. Fafard, Z. Wasilewski, J. McCaffrey, S. Raymond, and S. Charbonneau, *Appl. Phys. Lett.* **68**, 991 (1996).

¹⁹M. J. da Silva, A. A. Quivy, P. P. González-Borrero, N. T. Moshegov, and E. Marega Jr., *J. Cryst. Growth* **227/228**, 1025 (2001).

²⁰P. B. Joyce, T. J. Krzyzewski, G. R. Bell, B. A. Joyce, and T. S. Jones, *Phys. Rev. B* **58**, R15981 (1998).

²¹R. M. Thompson *et al.*, *Phys. Rev. B* **64**, 201302 (2001).

²²E. Moreau, I. Robert, J. M. Gérard, I. Abram, L. Manin, and V. Thierry-Mieg, *Appl. Phys. Lett.* **79**, 2865 (2001).

²³G. S. Solomon, J. A. Trezza, and J. S. Harris, Jr., *Appl. Phys. Lett.* **66**, 3161 (1995).

²⁴J. L. Jewell, J. P. Harbison, A. Schere, Y. H. Lee, and L. T. Florez, *IEEE J. Quantum Electron.* **27**, 1332 (1991).

²⁵I. N. Stranski and L. Von Krastanow, *Sitzungsber. Preuss. Akad. Wiss., Phys. Math. Kl.* **146**, 797 (1939); or for a review, see, e.g., W. Seifert, N. Calsson, M. Müller, M.-E. Pistol, L. Samuelson, and L. R. Wallenberg, *Proc. Cryst. Growth Charact. Mater.* **33**, 423 (1996).

²⁶K. E. Khor and S. das Sarma, *Phys. Rev. B* **49**, 13657 (1994).

²⁷J. Tersoff and F. K. Le Goues, *Phys. Rev. Lett.* **72**, 3570 (1994).

²⁸J. Drucker, *Phys. Rev. B* **48**, 18203 (1993).

²⁹C. Priester and M. Lannoo, *Phys. Rev. Lett.* **75**, 93 (1995).

³⁰N. Moll, M. Scheffler, and E. Pehlke, *Phys. Rev. B* **58**, 4566 (1998).

³¹H. T. Dobbs, D. D. Vvedensky, and A. Zangwill, *Phys. Rev. Lett.* **79**, 897 (1997).

³²B. A. Joyce, J. L. Sudijono, J. G. Belk, H. Yamaguchi, X. M. Zhang, H. T. Dobbs, A. Zangwill, D. D. Vvedensky, and T. S. Jones, *Jpn. J. Appl. Phys., Part 1* **36**, 4111 (1997).

³³H. M. Koduvely and A. Zangwill, *Phys. Rev. B* **60**, R2204 (1999).

³⁴Ch. Heyn and C. Dumat, *J. Cryst. Growth* **227/228**, 990 (2001).

³⁵Ch. Heyn, *Phys. Rev. B* **64**, 165306 (2001).

³⁶J. A. Venables, G. D. Spiller, and M. Hanbücken, *Rep. Prog. Phys.* **47**, 399 (1984).

³⁷H. T. Dobbs, A. Zangwill, and D. D. Vvedensky, *Surface Diffusion: Atomic and Collective Processes*, edited by M. C. Tringdes (Plenum, New York, 1997).

³⁸J. P. Harbison, D. E. Aspnes, A. A. Studna, L. T. Florez, and M. R. Kelly, *Appl. Phys. Lett.* **52**, 2046 (1988).

³⁹T. Farrell, J. Armstrong, and P. Kightley, *Appl. Phys. Lett.* **59**, 1203 (1991).

⁴⁰V. Bardinal, R. Legros, and C. Fontaine, *Appl. Phys. Lett.* **67**, 244 (1995).

⁴¹F. Stern, *Phys. Rev.* **133**, A1653 (1964).

⁴²S. Gehrsitz, F. K. Reinhart, C. Gourgon, N. Herres, A. Vonlanthen, and H. Sigg, *J. Appl. Phys.* **87**, 7825 (2000).

⁴³B. Y. Zhang, G. Solomon, G. Weihs, and Y. Yamamoto, *J. Cryst. Growth* **251**, 777 (2003).

⁴⁴C. Santori, D. Fattal, M. Pelton, G. S. Solomon, and Y. Yamamoto, *Phys. Rev. B* **66**, 045308 (2002).

⁴⁵M. Pelton, C. Santori, J. Vučković, B. Y. Zhang, G. Solomon, J. Plant, and Y. Yamamoto, *Phys. Rev. Lett.* **89**, 233602 (2002).

⁴⁶N. Lütkenhaus, *Phys. Rev. A* **61**, 052304 (2000).

⁴⁷K. Inoue, E. Waks, and Y. Yamamoto, *Phys. Rev. Lett.* **89**, 037902 (2002).